Catalysis Today 224 (2014) 3–12

Contents lists available at ScienceDirect

Catalysis Today

journal homepage: www.elsevier.com/locate/cattod

A critical review of CO_2 photoconversion: Catalysts and reactors

Kimfung Li [a], Xiaoqiang An [a], Kyeong Hyeon Park [a], Majeda Khraisheh [b,*], Junwang Tang [a,*]

[a] Department of Chemical Engineering, University College London, Torrington Place, London WC1E 7JE, UK
[b] Chemical Engineering Department, Qatar University, University Road, PO Box 2713, Doha, Qatar

ARTICLE INFO

Article history:
Received 10 August 2013
Received in revised form
18 November 2013
Accepted 2 December 2013
Available online 1 January 2014

Keywords:
Carbon dioxide
Semiconductor photocatalysts
Photoreduction
Reactor

ABSTRACT

Photocatalytic conversion of CO_2 to either a renewable fuel or valuable chemicals, using solar energy has attracted more and more attention, due to the great potential to provide an alternative clean fuel and solve the problems related to the global warming. This review covers the current progress of photocatalytic conversion of CO_2 by photocatalysis over the metal oxides. A brief overview of the fundamental aspects for artificial photosynthesis has been given and the development of novel photocatalysts for CO_2 photoreduction has been discussed. Several key factors for high-efficiency CO_2 photoreduction and the recent development of photocatalytic reactor design for this artificial photosynthesis have also been highlighted.

1. Background

Global warming is considered to be one of the major environmental concerns that humankind is facing [1]. Carbon dioxide (CO_2) contributes largely to the global climate change because it is one of the main greenhouse gases that are present in the atmosphere. CO_2 takes part in raising the global temperature through absorption of infrared light and re-emitting it. International Panel on Climate Change (IPCC) predicted that atmospheric CO_2 level could reach up to 590 ppm by 2100 and the global mean temperature would rise by 1.9 °C [2]. The impact of greenhouse effect will be global and serious in many different aspects, such as ice melting at the Earth's pole, fast rising sea level and increasing precipitation across the globe [3]. Energy generation by fossil fuel combustion dominates CO_2 emission and fossil fuel will be inevitably depleting. Therefore it is urgent for the scientists to find a renewable energy resource to mitigate the effect of global warming as well as meet the increasing energy demand [4].

In principle, there are at least three routes of reducing the amount of CO_2 in the atmosphere, including direct reduction of CO_2 emission, CO_2 capture and storage (CCS), and CO_2 utilization [5–7]. Despite the increasing utilization efficiency of fossil fuels, to dramatically lower the CO_2 emission seems difficult due to the increasing population and demand for high quality of life. The capacity of CCS technology is also limited due to the environmental risk of leakage and the energy requirement for gas compression and transportation. During the past decade, growing concerns have driven research activities toward the artificial conversion of CO_2 into fuels or valuable chemicals, through thermochemical, biological, electrochemical or photocatalytic methods [8–10]. In the long term, artificial photosynthesis, photocatalytic conversion of CO_2 using solar energy is the most attractive route for the transformation of CO_2 [11,12]. The interest in such field has been aroused dramatically after several examples which demonstrated photoelectrocatalytic reduction of CO_2 to organic compounds in 1970s [13]. Especially, the pace has recently increased enormously, because of the promoting effect of advanced technologies (e.g. nanotechnology and in-site advanced characterization) on the development of novel photocatalysts.

This review covers the approaches and opportunities of the artificial photosynthesis driven by solar energy using CO_2 as the raw material, including both material design and reactor engineering. The basic processes for the photocatalytic synthesis will be presented first. A significant proportion of the review focuses on the rational design of metal oxide photocatalysts with enhanced photocatalytic activity and the critical factors for high-efficient photoconversion of CO_2. The recent development of photocatalytic reactors for the artificial photosynthesis is also highlighted.

2. Artificial photosynthesis and the major elements

Photocatalytic CO_2 conversion makes use of semiconductors to promote reactions in the presence of light irradiation which is

* Corresponding authors. Tel.: +44 02076792747.
E-mail addresses: m.Khraisheh@qu.edu.qa (M. Khraisheh), Junwang.tang@ucl.ac.uk (J. Tang).

0920-5861
http://dx.doi.org/10.1016/j.cattod.2013.12.006

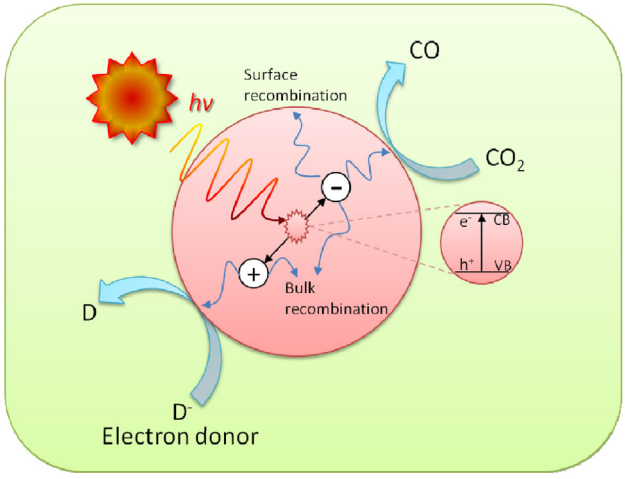

Fig. 1. Schematic diagram of photoexcitation and electron transfer process.

known as artificial photosynthesis. This review covers the artificial photosynthesis by metal oxide photocatalysts. The basic process can be summarized into three steps: (1) generation of charge carriers (electron–hole pairs) upon absorption of photons with suitable energy from light irradiation, (2) charge carrier separation and transportation, (3) chemical reactions between surface species and charge carriers [14,15]. Photocatalytic CO_2 conversion is a complicated combination of photophysical and photochemical processes. The redox reaction is initiated by photoexcitation when the energy of photons equal to or greater than the band gap of a semiconductor is received by a photocatalyst. Then the electrons are excited from the valence band (VB) to the conduction band (CB). VB is the highest energy band occupied by electrons and CB is the lowest in which there is no electron at the ground state [16]. As shown in Fig. 1, the electrons and holes undergo intra-band transitions. They can travel to the surface, combine at the trap sites (recombination process) through radiative or non-radiative pathways. Alternatively these electrons can travel to the surface of semiconductor and react with surface adsorbed species (CO_2 in this case), if recombination happens slower than the reactions during transitions [17].

However, not all the electrons reaching the surface can reduce CO_2 which is a thermodynamically inert and very stable compound. Compared with most of the reduction methods mentioned above which require high-energy input, either at high-temperature and/or under high pressure [18], photosynthesis does not require extra energy except solar irradiation. Photogenerated electrons at higher reduction potential level can offer driving force (also called over-potential) for the expected chemical reactions. The reduction potential measures the capability of a chemical specie to gain electrons. Species with a lower (more positive) reduction potential will gain electrons (i.e. be reduced) and those with a higher (more negative) reduction potential will lose electrons (i.e. be oxidized) [19]. In order to reduce CO_2 into carbon monoxide or hydrocarbons, electrons in the semiconductor are required to have more negative chemical potential, while for water oxidation, holes need to lie on more positive potential level. Eqs. (1)–(8) illustrate the pathways for the generation of solar fuels and the related potentials at pH = 7 [20].

Reaction		E^o (V vs NHE)
$CO_2 + 2e^- \rightarrow \bullet CO_2^-$	(1)	−1.90
$CO_2 + 2H^+ + 2e^- \rightarrow HCOOH$	(2)	−0.61
$CO_2 + 2H^+ + 2e^- \rightarrow CO + H_2O$	(3)	−0.53
$CO_2 + 4H^+ + 4e^- \rightarrow HCHO + H_2O$	(4)	−0.48
$CO_2 + 6H^+ + 6e^- \rightarrow CH_3OH + H_2O$	(5)	−0.38
$CO_2 + 8H^+ + 8e^- \rightarrow CH_4 + 2H_2O$	(6)	−0.24
$2H_2O + 4h^+ \rightarrow O_2 + 4H^+$	(7)	+0.81
$2H^+ + 2e^- \rightarrow H_2$	(8)	−0.42

From a thermodynamic point of view, formation of methane and methanol are more favorable in CO_2 reduction, since these reactions take place at lower potentials. However, the kinetic drawback makes methane and methanol formation more difficult than carbon monoxide, formaldehyde and formic acid because more electrons are required for the former reactions [21]. Moreover, the 2–8 electrons and protons reactions to obtain the desired products are extremely difficult. Due to the complicated nature of the inorganic photocatalyst surface, the interaction between photocatalyst and absorbed species may undergo a series of one-electron processes instead of a multi-electron, multi-proton process. Thus the actual redox potential required is determined by the reaction pathway. For example, if CO_2 reduction is initiated by single electron reduction of CO_2 to CO_2^-, the potential is around −1.9 V vs NHE. With such concern, being able to discharge multiple electrons with protons at a time is important to improve reaction efficiency. Thus, generating sufficient electron–hole pairs, separating charges efficiently and providing active catalytic sides are the paramount factors for CO_2 photoreduction.

Although photoreduction of CO_2 shows great potential [22,23], at present one of the greatest drawbacks is the low conversion efficiency. Herein, some of the key factors which limit the efficiency are listed: (1) mismatching between the absorption ability of semiconductor and the solar spectrum; (2) poor charge carrier separation efficiency; (3) low solubility of CO_2 molecule in water (approximately 33 μmol in 1 ml of water at 100 kPa and room temperature); (4) back reactions during reduction of CO_2; and (5) competition reaction of water reduction to hydrogen [24].

UV radiation only contributes less than 4% to the whole solar spectrum and 43% of the solar energy lies in the visible light region. To find a photocatalyst which can absorb visible light meanwhile has high enough CB position is one of the main goals of the research. An overpotential is necessary as a driving force for charge carrier transport and reactions, thus practical requirement for CO_2 conversion is usually greater than the theoretical energy required to produce the desired products [25].

Although directly matching the band gap of a semiconductor to the solar spectrum is challenging, several strategies have been used to improve the absorption ability of an inorganic photocatalyst. Doping with elements has been pursued to sensitize photocatalyst with a wide band gap, toward visible light absorption. As a broad and active topic, doping of photocatalysts with metal ions (Fe^{3+}, Zn^{2+}, W^{6+}, etc.) and non-metal ions (C, N, S, B, etc.) have already been widely studied in several review papers [26–30]. Therefore, a brief and general introduction is mentioned in this review. Doping does not only retard the fast charge recombination, but also introduce defect states (interband states or mid-gap levels) [31]. For example, it was reported that the narrowed band gap of a semiconductor after doping with non-metal ions (e.g. N or C) is ascribed to the mixing of p states of the dopants with O 2p states to form a new valance band [32]. However, the function of doping on CO_2 conversion is still arguable. Formation of semiconductor heterostructures is another effective way to enhance the light absorption and charge separation. Due to the band alignment, the band bending induces a built-in field, which drives the photogenerated electrons and holes to move in the opposite direction [33]. Semiconductor quantum dots (QDs) are also considered as an ideal choice for the coupled component in the heterostructures. In the presence of QDs, the visible light response of the photocatalysts is easily adjusted. In addition, QDs can also utilize hot electrons to generate multiple charge carriers when excited by a single high energetic photon, leading to an increased amount of the charge carriers [34]. Similarly, organic dyes are often used as sensitizers to enhance the visible light absorption of a semiconductor. Under irradiation, dyes can inject photoexcited electrons into the conduction band of the semiconductor. However, the electron transfer efficiency between

the dye sensitizer and the semiconductor depends on many factors, such as the LUMO level of the dye and the conduction band edge of semiconductor [35].

When CO_2 is reduced by the photogenerated electrons, utilization of an equal number of photogenerated holes should also be considered. Otherwise, the accumulation of the holes in a photocatalyst will increase the probability of charge recombination and shorten the lifetime of electrons. In addition, it is believed that holes could play a negative role in the photocatalytic reaction if they cannot be used efficiently, such as photocorrosion of the photocatalysts. The use of artificial electron donor to scavenge the holes is the most popular solution [36]. However, the process and energy used to synthesize the artificial electron donor needs to be taken into account since it may cause more CO_2 emission. Water is considered to be the ideal electron donor. Nevertheless, the large water oxidation potential is the main drawback, only very few photocatalysts that can reduce CO_2 and oxidize water simultaneously have been reported [37,38].

Competition from water reduction process by photogenerated electrons is also problematic when water is used as an electron donor. In comparison to most of the CO_2 reduction routes, reducing water is a relative easy process in term of kinetics and thermodynamics. In thermodynamics aspect, the reduction potential of water to hydrogen is 0.0 V (pH=0) which is more positive than CO_2 reduction to CO, formic acid and formaldehyde. In kinetics aspect, water reduction is a 2-electrons process, it is more facile than most of the CO_2 reduction which required 4–8 electrons. While CO_2 reduction is also limited by its low solubility in water, the water reduction does not suffer from the similar problem, thus the chance for electrons to meet and react with water is much higher than with CO_2. Although very little investigation has been conducted to address this problem, it is generally agreed that the reaction selectivity can be controlled by modifying photocatalysts' morphology, changing the exposed facets and introducing new reaction sides. It is believed that particular atom arrangement on the surface can be more favorable to absorb CO_2 molecule than water molecule on the surface. Two different morphologies of Cu_2O have been found to have dramatic difference in products' selectivity [39]. Co-catalyst loading has also claimed to be able to vary the reduction products' selectivity, Ag and Cu are commonly used as co-catalysts for CO_2 reduction whereas the loading of Pt or Au is more favorable for hydrogen production.

3. Metal oxide photocatalyst for CO_2 conversion

Inoue et al. demonstrated CO_2 photoreduction over various semiconductors under 500 W Xe or Hg lamp in the presence of electrical bias in 1979 [40]. The one or more converted products such as formaldehyde, formic acid, methanol and methane were detected on different materials. Since then, there have been some reports on CO_2 photoconversion. Compared to the material development for the analog process, photocatalytic water splitting, fewer materials have been developed for photoreduction of CO_2. Many photocatalysts that are acknowledged as good candidates for water splitting cannot reduce CO_2 due to the kinetic difficulty. Although some sulfides and nitrides have been reported to be active for CO_2 conversion, the metal oxides are more preferable [41,42], due to their potential advantages over sulfides and nitrides, e.g. relatively safe to handle, fairly low cost and considerably stable, thus particular attention is paid to photoreduction of CO_2 using metal oxide photocatalysts below.

4. Titanium dioxide

TiO_2 is the most investigated photocatalyst for artificial photosynthesis. Pure titanium oxide has three common mineral phases, including anatase, brookite and rutile. Photocatalytic conversion of CO_2 over single-phase or mix-phase TiO_2 has been widely investigated. The phase structure and surface properties of TiO_2 have a significant influence on the efficiency of photoreduction. Liu et al. compared the photoactivity for CO_2 photoreduction to CO and CH_4 over TiO_2 in three different phases [43]. It was found the brookite had the highest CO and CH_4 yield. Although rutile showed smallest band gap which had the strongest visible light absorption, it was the least active photocatalyst. The application of mix-phase TiO_2 was more attractive. It has demonstrated an enhanced visible light harvesting ability and the anatase-dominated mixed phase was benefited to CO_2 photoreduction [44]. The enhancement was also attributed to the junction effect between rutile and anatase resulting an efficient charge separation.

Morphology of TiO_2 has significant influences on the photoactivity of CO_2 reduction. TiO_2 nanorods and nanotubes have attracted much attention due to their large surface area, reduced grain boundaries and facile charge transport paths of 1-D nanomaterials [45]. For example, mixed-valence state Pt dispersed TiO_2 nanotube (TNT) was used for CO_2 photoreduction [46]. The Pt nanoparticles were uniformly distributed on TiO_2 nanotube (TNT) through deposition of Pt complex. Due to the synergetic effect of tubular morphology and the mixed valence Pt nanoparticles, CO_2 adsorption ability of Pt/TNT was greatly improved. The in situ FT-IR study also showed that Pt/TNT was extremely active toward the hydrogenation of CO_2 to methane at 100 °C. Zhang et al. further optimized the Pt loading amount, reaction temperature and the ratio of H_2O/CO_2 in the reaction. The optimal condition for CO_2 reduction was determined to be: 0.15 wt% Pt-loaded TNT with H_2O/CO_2 molar ratio of 0.9:1 at 343 K [47]. The influence of annealing temperature on the specific photocatalytic reactions was also studied by other groups. Vijayan et al. reported that TNT calcined at 400 °C had the best photocatalytic performance for converting CO_2 to methane [48]. On the other hand, Schulte et al. showed that low-temperature calcination (550 °C) resulted in the lowest production (0.26 $\mu mol\,m^{-2}\,h^{-1}$) whereas samples fabricated at 680 °C had the highest production rate of 0.79 $\mu mol\,m^{-2}\,h^{-1}$ owing to the increased visible light harvesting [49]. The results are not aligned which may be due to different reaction conditions in different labs and raises a serious question how to reasonably compare the activity of a photocatalyst reported by different groups. Varghese et al. carried out an outdoor experiment over nitrogen-doped TNT arrays under actual sunlight. 52% of nanotube surface was covered by Cu and the rest was coated by Pt. A series of hydrocarbons (methane, olefin branded paraffin and other alkane) and CO were detected. Their formation rates were found superior to the TNT without co-catalyst or TNT with single co-catalyst. The maximum production rate was reported to be 111 $ppm\,cm^{-2}\,h^{-1}$ [50]. Most recently, Zhang et al. reported four-fold increase of CO_2 conversion rate by filling Cu–Pt binary co-catalyst inside the nanotube cavity, the SEM images of which are shown in Fig. 2. When $Cu_{0.33}$–$Pt_{0.67}$/TNT was used to photoreduce diluted CO_2 (1% in N_2), hydrocarbons (CH_4, C_2H_4, and C_2H_6) production rate of 6.1 $mmol\,m^{-2}\,h^{-1}$ was achieved under AM 1.5 illumination [51]. Copper decorated TiO_2 nanorod films have also been used for CO_2 photoreduction. With addition of Cu nanoparticles, the CH_4 production rate (2.91 $ppm\,g^{-1}\,h^{-1}$) was about two time higher than that of bare titania films, this might be due to the enhanced electrons and holes' separation or surface plasmonic effect induced by the metal nanoparticles [52].

The unique pore structure and large surface area of mesoporous materials have let their application toward CO_2 photoreduction rather attractive. Noble metals (Pt, Au, and Ag) loaded nitrogen doped mesoporous TiO_2 have been used for converting CO_2 into methane under visible light irradiation. Their photocatalytic activities followed the descended order of $Pt/TiO_2 > Au/TiO_2 > Ag/TiO_2$. The reason for this was ascribed to the higher working function of

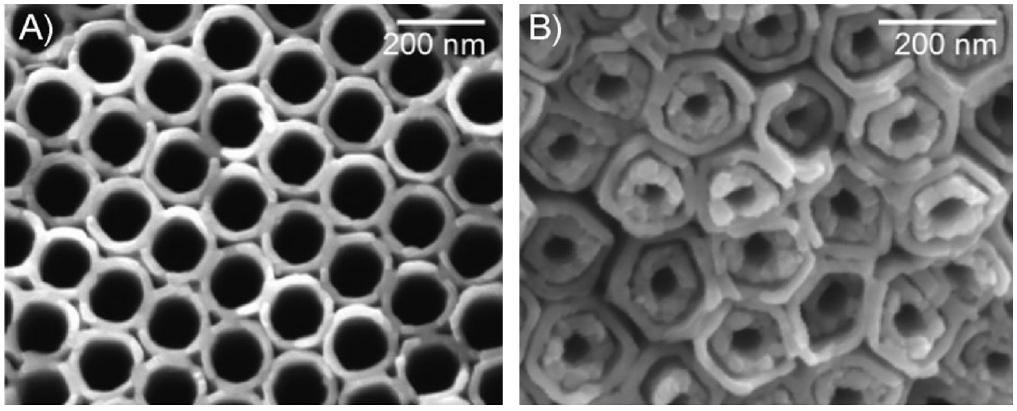

Fig. 2. SEM images of (a) bare TiO_2 nanotube and (b) Cu- and Pt-loaded TiO_2 nanotube. Reproduced from Ref. [51].

Pt, which facilitated the transfer of photogenerated electrons from TiO_2 to noble metal particles [53]. The optimum loading amount of Pt was found to be 0.2 wt%, with methane yield of 2.9 μmol m^{-2} h^{-1}.

Dispersion of photocatalysts is noted to be another important factor for efficient photoreduction of CO_2. Photocatalysts immobilized in the zeolite or silicate frameworks are usually highly dispersed, which offers unique pore structure and ion exchange capacity for reactions [54,55]. It was reported that titania anchored on zeolite had high selectivity for methanol formation. Selectivity of reaction products could be controlled by the addition of the co-catalysts, such as Pt is beneficial for formation of methane rather than methanol [56]. Ti-containing porous SiO_2 films could convert CO_2 into CH_4 and CH_3OH with the quantum yield of 0.28%, which was superior to dense phase TiO_2 particles. The enhanced efficiency was ascribed to the ligand-to-metal charge transfer, which was caused by the excitation of isolated Ti centers by UV light [57]. Furthermore, Ulagappam et al. used Ti silicate molecular sieves to convert CO_2 into formic acid, acetic acid and CO and the possible reaction paths were investigated by FT-IR measurements [55]. The photoreduction of CO_2 over TiMCM-41 molecular sieves was carried out under laser light. The double electron transfer of CO_2 generated carbon monoxide, which was directly proportional to the power of the laser [58].

4.1. Non-titanium photocatalysts

Since the field of artificial photosynthesis is advancing fast, the family of non-titanium photocatalysts for CO_2 reduction is in parallel developing and updating in a rapid speed. Several types of metal oxide and mixed metal oxide semiconductors have been reported, including ZrO_2, Ga_2O_3, Ta_2O_5, $SrTiO_3$, $CaFe_2O_4$, $NaNbO_3$, $ZnGa_2O_4$, Zn_2GeO_4 and $BaLa_4Ti_4O_{15}$, etc. [59–61]. As most of them have a large band gap, which can provide great overpotential for the reaction, these metal oxides usually are UV active.

ZrO_2 is a popular photocatalyst owing to its high CB position, its photogenerated electrons have large driving force for CO_2 reduction. Sayama et al. investigated 1% Cu loaded ZrO_2 to reduce CO_2 using $NaHCO_3$ aqueous solution as CO_2 source. The selectivity for CO was about 10% and H_2 was the main reduction product indicating that electrons were tended to reduce protons in water [62]. Kohno et al. and Lo et al. both investigated photoconversion of CO_2 over ZrO_2 in the presence of H_2 under UV illumination. CO was found to be the sole product of the reaction, with the yield of 0.70 μmol g^{-1} h^{-1} and 0.51 μmol g^{-1} h^{-1} respectively [63–65]. Kohno et al. further investigated the reaction mechanism. As reported, ZrO_2 reduces CO_2 molecules into CO_2^- anion radicals, which subsequently reacts with H_2 to form formate ($HCOO^-$) on the surface. The reaction between formate and another CO_2 molecule led to the formation of CO [66]. Similar results were also achieved when CH_4 was used instead of H_2, except the formation of extra carbonaceous residue (CH_3COO^-) in the reaction [67]. When H_2 was used as the reductant, the CO production rate was about 0.17 μmol h^{-1}, followed by 3.3 μmol of CO additionally released upon heating. In contrast, the CO yield was about 0.14 μmol h^{-1} in the presence of CH_4 reductant and further 1.5 μmol CO, 0.2 μmol H_2 and 0.2 μmol CH_4 were collected upon heating [68].

$ALa_4Ti_4O_{15}$ (A = Ca, Sr, and Ba), with a layered perovskite structure and band gap of 3.79–3.85 eV, have been used for CO_2 photoreduction. Iizuka et al. found that $ALa_4Ti_4O_{15}$ can reduce water without additional reductant. However, hydrogen was the preferential reduction product [69]. $BaLa_4Ti_4O_{15}$ was determined to be the most active photocatalyst and its selectivity was shifted toward CO_2 reduction after introducing Ag metals on the surface. The effect of co-catalyst loading methods on the photoactivity has also been investigated. The photoactivity has been found in descending order: Ag production using liquid-phase reduction by $NaPH_2O_2$ > impregnation and subsequent H_2 reduction > impregnation > in situ photodeposition. The advanced performance was ascribed to the small particle size of Ag metals and the uniform distribution of co-catalysts on the surface. The optimal loading amount was determined to be 2.0 wt% Ag-loaded $BaLa_4Ti_4O_{15}$, with maximum H_2, O_2, CO and HCOOH yields of 10 μmol h^{-1}, 16 μmol h^{-1}, 22 μmol h^{-1} and 0.7 μmol h^{-1} [69].

For most of the other photocatalysts, O_2 usually cannot be detected while in the absence of artificial electron donor, which raises concerns about the role of holes in the photocatalytic reaction. Xie et al. employed self-doped $SrTiO_{3-\delta}$ for CO_2 photoreduction under visible light. $SrTiO_{3-\delta}$ was prepared through a carbon-free combustion method followed by the heat treatment in argon, which could create sufficient oxygen deficiencies and high spin Ti^{3+} in the material. Because of the enhanced CO_2 adsorption and the reduced band gap, methane production rate over 0.3 wt% Pt-loaded $SrTiO_{3-\delta}$ reached 0.25 μmol m^{-2} h^{-1}. The photogenerated holes were thought to be consumed by the oxidization of photocatalyst from Ti^{3+} to Ti^{4+}. The assumption was partially backed up by the factor that photoactivity of $SrTiO_{3-\delta}$ dramatically decreased after 10 h. In order to regenerate Ti^{3+}, the photocatalyst needed to be recovered by heating at 1200 °C in argon [70]. Although oxidation of photocatalysts was seldom mentioned in the other reports, which raises a serious issue about the photocatalyst stability, decrease of photocatalyst performance was frequently observed with prolonged reaction time.

Several non-titanium metal oxides nanomaterials with special morphologies have also been developed for photoreduction of CO_2. $NaNbO_3$ nanowire was fabricated through the hydrothermal synthesis followed by the heat treatment. The CH_4 evolution rate

of nanowires reached 653 ppm g^{-1} h^{-1}, much higher than that of bulk $NaNbO_3$ particle fabricated through solid-state reaction (22 ppm g^{-1} h^{-1}) [71]. Yan et al. studied the photoreduction of CO_2 into CH_4 over $ZnGa_2O_4$. The CH_4 production rate of mesoporous $ZnGa_2O_4$ (5.3 ppm h^{-1}) was superior to $ZnGa_2O_4$ obtained by solid-state reaction (trace amount). The CH_4 yield was further increased to 50.4 ppm h after loading 1 wt% RuO_2 on mesoporous $ZnGa_2O_4$ [72]. Liu et al. compared the photoactivities of Zn_2GeO_4 nanoribbon and bulk Zn_2GeO_4 prepared through solid-state synthesis. In the presence of 1 wt% RuO_2 and 1 wt% Pt, the optimal CH_4 yield of Zn_2GeO_4 nanoribbon was 25 μmol g^{-1} h^{-1}, which is much superior to bulk Zn_2GeO_4 (only trace amount of CH_4 detected) [73]. Although the overall water photooxidation and photoreduction by pristine Zn_2GeO_4 and RuO_2-Pt-loaded Zn_2GeO_4 have been observed during photocatalytic water splitting, the yields of H_2 and O_2 were not determined in the report [74]. The photoactivity of highly porous Ga_2O_3 for CO_2 reduction was four times higher than that of commercial bulk Ga_2O_3, without the addition of co-catalyst and sacrificial reagent [75]. It was reported that the direct conversion from CO_2 to CH_4 was realized in the absence of CO intermediates, while holes were consumed by water to produce H^+ and OH•. The enhanced performance of porous Ga_2O_3 was attributed to the two-fold increase of surface area and the tripled CO_2 adsorption ability. Tanaka et al. carried out the photoreduction of CO_2 over bulk Ga_2O_3 in the absence of H_2O, using H_2 as reductant. CO was formed instead of CH_4, with the yield of 10.96 μmol after 2 days. It was noticed that about 7.3% of surface adsorbed CO_2 was converted [76]. Subsequently, photoreduction of CO_2 over $ATaO_3$ (A = Li, Na and K) was investigated under similar conditions. $LiTaO_3$ showed the highest activity for CO production (0.42 μmol g^{-1} in 24 h), while $KTaO_3$ presented the lowest yield [77]. $KTaO_3$ have the smallest band gap among those three tantalate compounds and it have a suitable VB that can oxidize water [78]. It can potentially reduce CO_2 using water as hole scavenger. To enhance its photoactivity, $KTaO_3$ nanoplate were synthesized in solvothermal reaction [79]. CO, H_2 and O_2 were detected without electron donor or electric bias in our reaction. A seven times increase in CO yield over $KTaO_3$ nanoplate compared to the conventional $KTaO_3$ was achieved. The increase was ascribed to the short electron diffusion distance to the surface in the thin plate-like particle. Matsumoto et al. reported the conversion of CO_2 into methanol and formaldehyde over p-type $CaFe_2O_4$ in the solution of sodium hydroxide [80].

Developing visible-light-driven semiconductors for artificial photosynthesis is one topic of great interest with practical importance. Besides the self-doped $SrTiO_{3-\delta}$, unfortunately, only a few candidates with both visible light response and acceptable photoactivity have been reported even in the presence of electron donor, such as Cu_2O, $BiVO_4$, $LaCoO_3$ $InTaO_4$ and N-doped Ta_2O_5.

Since Punchihewa discovered Cu_2O for photocatalytic reduction of CO_2 in 1989, Cu_2O has been an attractive visible-light-driven photocatalyst for artificial photosynthesis [81]. However, stability of Cu_2O is still the biggest drawback to its application in photosynthesis, as Cu_2O can be easily oxidized or reduced by photogenerated charge carriers. Punchihewa et al. found that formation of formaldehyde and methanol reached maximum concentrations in 30 min and 45 min respectively. After that, the product concentrations declined, because the back reaction by photogenerated holes became faster than the reduction of CO_2. More recently, photocatalytic reduction of CO_2 into methanol over Cu_2O/SiC was rendered by Li et al. [82]. The photocatalytic performance of SiC nanoparticles was improved by the modification with Cu_2O. As a result, the yield of methanol increased from 153 to 191 μmol g^{-1}. Although a linear increase of methanol yields over Cu_2O/SiC was shown, the chemical state of Cu_2O after the reaction was not mentioned. Thus, the problem of stability could not be excluded, as the enhancement could be ascribed to Cu metal or thin layer of CuO on SiC. For the practical application of Cu_2O in the field of solar energy conversion, new strategies to form heterostructured protection layer are highly desirable. For example, with the protection of Al-doped ZnO and TiO_2 nanolayers, the stability of Cu_2O electrodes were significantly improved for water reduction even if it was not tested for CO_2 conversion [83]. It was also reported that the existence of robust carbon layer could improve the stability of Cu_2O [84]. In our previous research, it was found that improved CO conversion yield could be achieved by coupling Cu_2O with RuO_2, forming a heterojunction which retarded charge recombination [39].

Zou et al. first reported the application of Ni-doped $InTaO_4$ for overall water splitting in the absence of scavenger under visible light irradiation. With the aid of RuO_2 or NiO_x as a co-catalyst, H_2 and O_2 production in the stoichiometric ratio was achieved. The quantum yield at 402 nm was reported to be 0.66% [85]. Later, Pan et al. used $NiO_x/InTaO_4$ to convert CO_2 into methanol. The role of NiO_x was ascribed to attract electrons and to provide active reaction sites. With a proper deposition method (reduction followed by oxidation), the maximum methanol yield was 1.394 μmol g^{-1} h^{-1} [86]. It should be noted that methanol was the only product in the reaction. Other carbohydrates, CO, hydrogen or oxygen were not mentioned. Wu et al. prepared $InTaO_3$ nanoparticles with the size of 17.7 nm by sol–gel method. Compared to $InTaO_3$ fabricated by solid-state synthesis, 37.5% increase was achieved during the conversion of CO_2 into methanol [87]. The conversion efficiency of CO_2 into ethanol over monoclinic $BiVO_4$ was found to be 17 times higher than tetragonal $BiVO_4$. The enhancement was ascribed to the binding of CO_3^{2-} to the Bi^{3+} sites by Bi—O bonds [88]. Alcohols are widely used as hole scavengers, which can efficiently extract the photoinduced holes, subsequently oxidize themselves into CO_2, CO, etc., therefore there is an argument about the detected products which may be produced by the surface organic contaminants absorbed during photocatalyst synthesis. Jia et al. studied the photoreduction of CO_2 over C and Fe co-doped $LaCoO_3$ under 125 W Xe lamp with 400 nm long pass filter. For C-$LaCo_{0.95}Fe_{0.05}O_3$, formaldehyde and formic acid were collected with the maximum yield of 19 μmol g^{-1} h^{-1} and 128 μmol g^{-1} h^{-1} [89].

Doping is an efficient way to enhance the visible light response of photocatalysts. Visible light driven CO_2 conversion into formic acid was realized over a wide bandgap material (Ta_2O_5) when modified by nitrogen doping. In the presence of ruthenium complex, hybrid photocatalysts showed the quantum yield of 1.9% under visible light (405 nm) [90]. Suzuki et al. synthesized nitrogen doped mesoporous Ta_2O_5 spheres, which exhibited enhanced visible light response than N-doped Ta_2O_5 fine particles [91].

In the past few years, graphene-based semiconductor photocatalysts have attracted a wide interest in the field of solar fuel production. It has been reported that coupling metal oxide with graphene can not only enhances the visible light absorption, but also improves the efficiency of charge separation, which are crucial factors for visible-light-driven photocatalytic reduction of CO_2. The conversion rate of CO_2 into methanol over NiO_x loaded Ta_2O_5/1.0 wt% graphene composites reached 0.5 μmol g^{-1} h^{-1}, which was 3.4 times higher than the corresponding photocatalyst without graphene. The enhanced conversion efficiency was attributed to the superior conductivity of graphene and the facilitated charge transfer from Ta_2O_5 to active site of co-catalysts [92]. In situ simultaneous reduction-hydrolysis technique was developed to fabricate TiO_2/graphene hybrid nanosheets. The synergistic effect of the surface-Ti^{3+} abundant TiO_2 and graphene favors the generation of C_2H_6, and the yield of the C_2H_6 increases with the content of incorporated graphene [93]. Hollow spheres consisting of titania nanosheets and graphene nanosheets were fabricated by a layer-by-layer assembly method. As shown in Fig. 3, the sufficiently compact stacking of ultrathin $Ti_{0.91}O_2$ with graphene

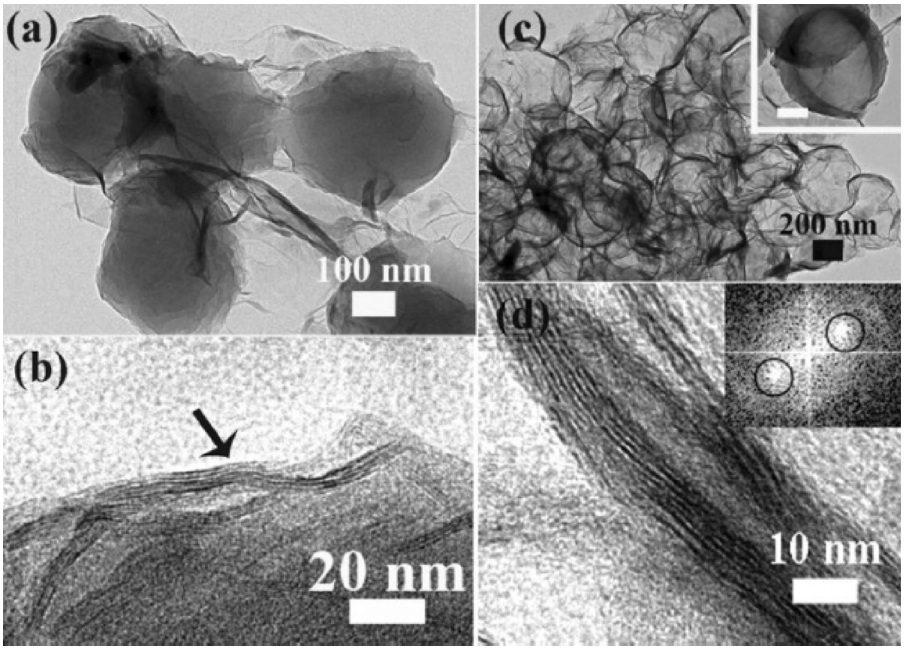

Fig. 3. TEM images of (a and b) PMMA spheres coated with $(PEI/Ti_{0.91}O_2/PEI/GO)_5$, (c and d) $(G\text{-}Ti_{0.91}O_2)_5$ hollow spheres. Reproduced from Ref. [94].

nanosheets resulted in the nine times improvement [94]. However, scientific research is highly desirable to understand the underlying mechanism of graphene-based photocatalysts for CO_2 reduction, as several aspects showed significant influence on the efficiency of composites. For example, Liang et al. found that nanocomposites based on the less defective solvent-exfoliated graphene exhibited a significantly larger enhancement during the photoreduction of CO_2 to CH_4, compared to solvent-reduced graphene oxide [95]. The fabrication of high quality graphene-based composites is still challenging and more efficient strategies would need to be developed to address these issues.

5. Important factors for photoreduction of CO_2

It is difficult to compare the activities of different photocatalysts reported by different groups by only considering the conversion rate or quantum efficiency due to the differences among preparation methods and in particular test conditions. However, it is generally agreed that several aspects can be considered to improve the photocatalytic performance of semiconductors.

The particle size of photocatalyst has great effect on the efficiency of CO_2 photoreduction. Decreasing particle size can often results in the larger surface area of the photocatalysts, which serves more active reaction sites for CO_2 adsorption. The photocatalysts with smaller particle size also benefit from the shorter transfer pathway for charge carriers to reach its surface. However, the smaller the particle size is, the more the particles' boundary, which may influence the communication between these particles and thus leads to a lower activity. Ye et al. prepared $NaNbO_3$ by hydrothermal method and polymerized complex method separately. $NaNbO_3$ nanoparticles fabricated by the polymerized complex method exhibited much larger surface area than the hydrothermal products, which were 38 $m^2\,g^{-1}$ and 1.7 $m^2\,g^{-1}$ respectively. As a result, treble and sextuple enhancements of O_2 and H_2 production rate were achieved [96]. Several kinds of nanomaterials with typical morphologies show great impact on the efficiency of CO_2 reduction, such as one-dimensional nanorods and nanotubes with unique charge transfer paths, mesoporous nanostructures with considerable large surface area.

Besides particle size, controlling the facets of photocatalysts has been proved to be an efficient way to improve the activity of photocatalysts. Our preliminary results showed that the photocatalytic reduction preference shifts from H_2 (water splitting) to CO (CO_2 reduction) by controlling the exposed facet of Cu_2O. The low index facets {100} exhibit higher activity for CO_2 photoreduction than high index facets {111} [39].

Loading co-catalysts on the surface of photocatalysts is another commonly used procedure to achieve substantial enhancement on both conversion efficiency and products' selectivity. It is generally known that the photoreduction reaction can be improved by loading noble metal nanoparticles. On the other hand, metal oxide nanoparticles are found to favor the oxidation reaction. The choice of co-catalyst is crucial. Some noble metals are particular active toward water reduction while some are more suitable for CO_2 reduction. This is due to the co-catalysts providing active catalytic sites for reduction of different absorbed species. The co-catalysts also extract the photogenerated electrons or holes to prolong the lifetime of the charge carriers. Although metal oxide does not provide reduction catalytic reaction side, loading it on photocatalyst may still increase the reduction products' yield, since it will extract hole and extend the lifetime of electrons for reduction reaction (e.g., CO_2 reduction over $Cu–RuO_x$). In addition, electron accumulation on co-catalyst allows the discharge of more than one electron at a time, facilitating the multi-electron CO_2 reduction processes.

The choice of the co-catalysts varies from different photocatalysts for reaching their best photoactivity. To date, the co-catalyst application strategy for CO_2 reduction is mainly focused on CO_2 reduction co-catalysts. However, there are other strategies used in photocatalytic or photoelectrocatalytic (PEC) water splitting system, such as (1) oxidation co-catalysts for hole removal from photocatalyst and (2) binary co-catalysts system for both reduction and oxidation reactions.

Noble metals Pt, Cu and Ag are the three most commonly used co-catalyst for CO_2 photoreduction. Loading Pt co-catalyst

generally benefits the formation of CH_4 whereas CO is more preferable in the presence of Cu or Ag. Yamakata et al. reported that the recombination of electrons and holes was greatly retarded when Pt was loaded on photocatalysts [97]. Pt loaded TiO_2 and Zn_2GeO_4 have been used for photocatalytic CO_2 reduction, CH_4 was found to be the only reduction product [73,98]. However. Pt is also a well-known co-catalyst for water reduction. In one of our experiments, Pt loaded $KTaO_3$ was used to photoreduce CO_2 under UV irradiation. It was found the hydrogen yield was dramatically increased compared to pristine $KTaO_3$, while only trace amount of CH_4 was produced [79]. Thus, how to controlling the competition reaction of water reduction is important, as Pt may facilitate the activation of H_2O. To overcome the problem, Zhai et al. used a Pt/Cu_2O binary co-catalyst with a core/shell structure for CO_2 reduction over TiO_2. H_2, CO, CH_4 and O_2 were formed and the presence of Cu_2O shell attributed to the higher yield of CO. Pt co-catalyst decreased the selectivity of CO_2 reduction, whereas the selectivity increased from 60 to 80% by loading Cu_2O shell. It was proposed that the Cu_2O shell provided the preferential reaction sites for CO_2 conversion while the Pt core was served as electron sink to "collect" the photogenerated electrons from TiO_2. Therefore, the deposition of a Cu_2O shell on Pt markedly suppresses the reduction of H_2O to H_2, a competitive reaction with the reduction of CO_2 [99].

Copper and silver have been widely used as co-catalysts for CO_2 reduction. Owing to the effect of Cu as electron trapper to prohibit the recombination of electron–hole pairs, the loading of Cu to $BaLa_4Ti_4O_{15}$, ZrO_2, SiC and TiO_2 could efficiently enhance their photoactivities [100–103]. Peterson et al. investigated the mechanism of Cu as co-catalyst for CO_2 reduction. They found the weak bonding of CO to copper surface prevented the formation of adsorbed CO to CHO, which was a crucial intermediate for the hydrocarbon [104]. Ag-loaded $BaLa_4Ti_4O_{15}$, $SrTiO_3$ and TiO_2 have been utilized for CO_2 photoreduction [105,106]. It is worth to point out that the addition of Ag, Cu and NiO_x to $BaLa_4Ti_4O_{15}$ as a co-catalyst resulted in the photoreduction of CO_2, whereas only H_2 and O_2 were detected for pristine $BaLa_4Ti_4O_{15}$. Enhancements in the production of H_2 and O_2 were also observed when Ru and Au were loaded, but CO could not be detected. These results indicate that both Cu and Ag can function as reaction sites for CO_2 reduction and electron trapper.

Although noble metal co-catalysts are well-known for improving photocatalytic activity, development of low-cost co-catalyst seems extremely important. To date, several types of non-noble-metal co-catalysts, such as NiO, Co–Pi, MoS_2 and WS_2, have been engaged in photocatalytic reactions [107–111]. Kudo et al. first reported the overall water splitting using Ni/NiO_x-loaded La doped $NaTaO_3$ in 2000. Later, NiO was employed as a co-catalyst on $InTaO_3$, $Sr_2Nb_2O_7$ and $Sr_2Ta_2O_7$, etc. Co–Pi was first reported for boosting water oxidation in 2008, which could significantly lower the overpotential required for water oxidation. Recently, Durrant et al. studied the dynamics of photogenerated charge carriers in Co–Pi loaded Fe_2O_3 by transient absorption spectroscopy. The improvement was ascribed to the increased life time of photogenerated holes by at least 3 orders of magnitude [112]. Recently, Wang et al. reported the addition of MgO on TiO_2 to enhance the chemisorption of CO_2 onto the catalyst surface greatly accelerated the photocatalytic reduction of CO_2 to CH_4 [113]. Molybdenum and tungsten sulphides have also been reported for water reduction over CdS, which may serve as potential non-noble metal co-catalysts for CO_2 reduction [114,115]. Enhancement of overall water splitting was also found over $NaTaO_3$ coupled with $[Mo_3S_4]^{4+}$ [116]. Nevertheless, the stability and safety issues of metal sulfide compounds may limit their practical applications.

In conclusion, several factors are important for a good photocatalyst, e.g. small particle size, high surface area and right exposing facets besides long lived charge carriers. Furthermore, even though the photocatalyst is suitable for CO_2 reduction, the photogenerated electron and hole may recombine if there are no suitable active/reaction sites available on the surface of the light harvesting semiconductor. Therefore, it is essential to introduce active catalytic sites for CO_2 reduction on the surface of semiconductor by loading co-catalysts.

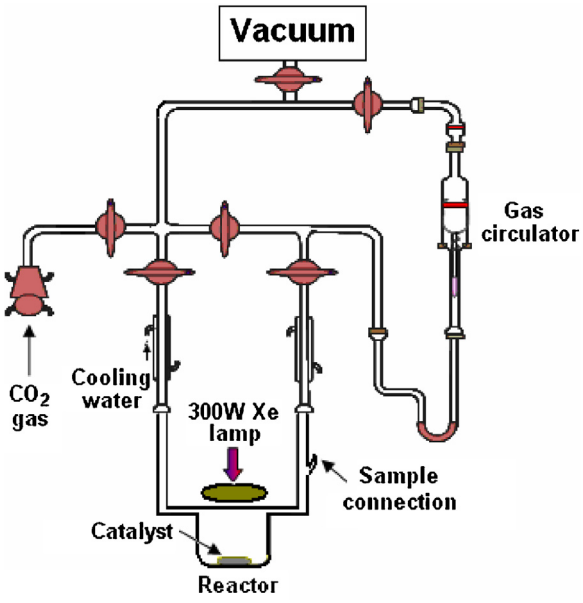

Fig. 4. Fluidised bed batch reaction setup for CO_2 photoreduction. Reproduced from Ref. [72].

6. Development of photoreactors

Photoreactor development is an engineering approach to enhance efficiency of CO_2 conversion. It involves advancing the light harvesting technique, reducing loss of photon, improving products separation and influencing charges carrier recombination as well as the reactive surface area of a photocatalyst. The reactor system can be grouped into two categories: fluidised bed reactor and fixed bed reactor. Fig. 4 shows a fluidised bed batch reactor system, it is the most commonly used system. Fluidised bed reactor is operated as a batch process in two-phase heterogeneous system. The photocatalysts are suspended in a fluid-like state providing highly dispersed photocatalysts with agitation by magnetic stirrer to prevent catalyst sedimentation. Reaction starts with filling CO_2 into the sealed reactor (some may firstly remove air by vacuum to improve the purity), then light irradiates from the top of the reactor. The sample is taken in a fix time interval by gastight syringe or on-line automatic sampling system. It should be noted the types of lamp, reactor size and amount of water and photocatalyst used may vary in different systems.

The light harvesting efficiency can be increased by changing the lamp position. As shown in Fig. 5, in an inner irradiation cell, the lamp is placed inside the reactor. Hence the light loss by reflection is minimized.

Wu et al. also developed fiber reactor to reduce the loss of light. CO_2 photoreduction was performed where photocatalyst was coated on optical fiber (the fixed bed) and the fluid was guided to form a plug-flow-state [105]. As shown in Fig. 6, the fiber served as a medium to deliver light effectively and uniformly to the surface of a photocatalyst. When light travels inside the fiber, part of the light is reflected and transmitted along the fiber and the rest of the light penetrates and excites the TiO_2 layer at the interface. NiO_x-loaded $InTaO_4$ photocatalyst has been used to compare fiber reactor and conventional reactor for CO_2 photoreduction. The methanol yield

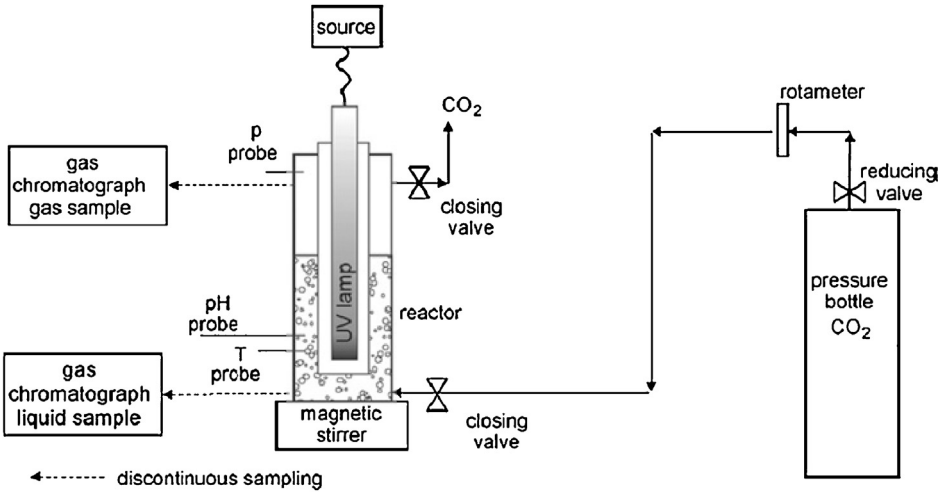

Fig. 5. Illustration of inner irradiation cell for CO_2 photoreduction.
Reproduced from Ref. [117].

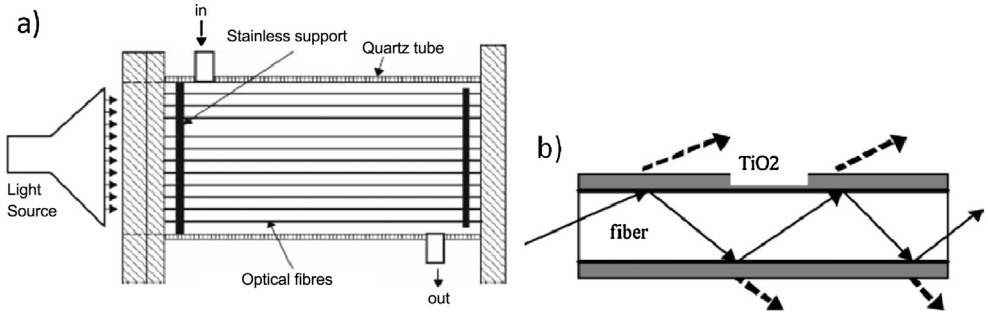

Fig. 6. (a) Schematic illustration of an optical-fiber photoreactor and (b) the schematic diagram of light transmission and spread in a TiO_2 coated-optical fiber.
Reproduced from Ref. [105].

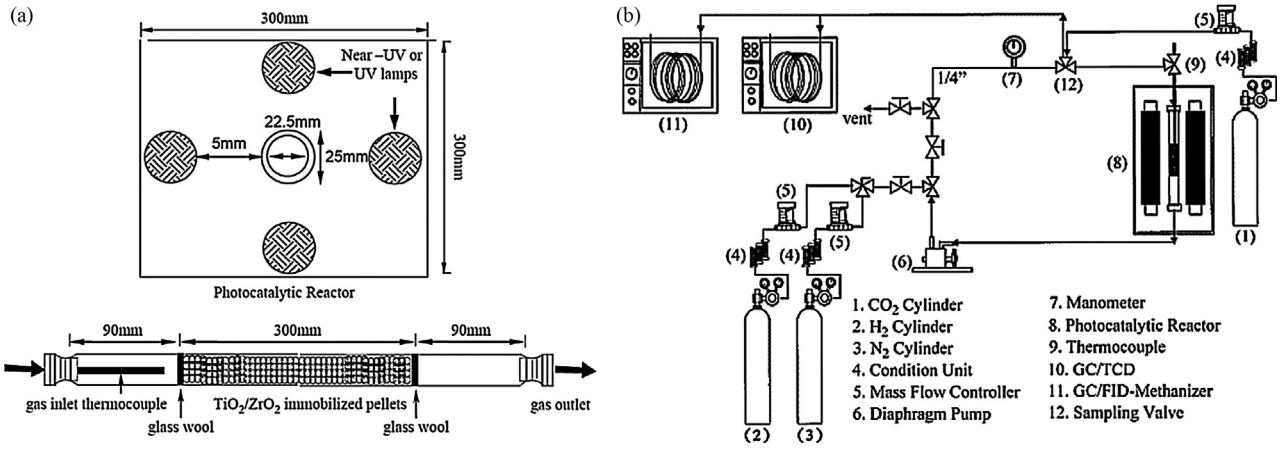

Fig. 7. (a) Schematic illustration of a photoreactor and (b) the schematic diagram of a close circulated system setup.
Reproduced from Ref. [65].

in optical fiber reactor was 14 times higher than the yield in the conventional batch reactor [60]. In another report, CO_2 photoreduction was conducted over Pd and Rh-loaded TiO_2 in an optical fiber reactor. Quantum efficiency (0.049%) achieved in the optical fiber reactor is higher than that in a conventional batch reactor (0.002%) [118].

Lo and co-workers reported a circulation photocatalytic reaction system using a fixed bed for CO_2 conversion, which is shown in Fig. 7. The circulation reactor has advantages over the conventional batch reactor in providing a high uniformity of the gas concentrations distribution inside the reactor and shortening the reaction time. In addition, the immobilized photocatalyst offers high specific reactive surface area.

Ichikawa and Doi reduced CO_2 using a Nafion film as a proton separator coated by TiO_2 and ZnO/Cu on different sides in the presence of an external bias [119]. As shown in Fig. 8, the system consists

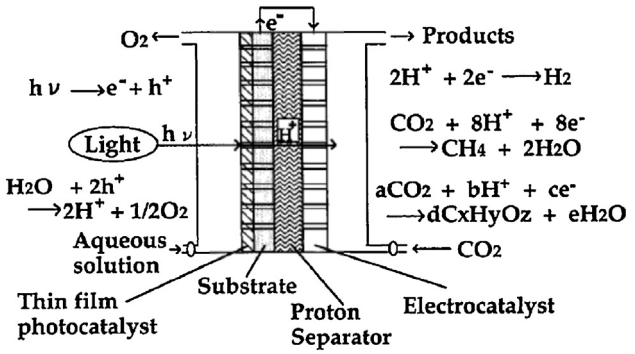

Fig. 8. Schematic illustration of a photoreactor equipped with proton separator. Reproduced from Ref. [119].

Fig. 9. Photo of solar concentrator employed in Wu et al. study. Reproduced from Ref. [121].

of a thin film TiO_2 and an electrocatalyst which were coatedon a Nafion film. The reactor separated the production of oxidation and reduction products to avoid further reactions between products as well as reduce energy required in subsequent purification. Furthermore, the use of proton membrane reduced the chance of the back reaction between proton and O_2. Recently, Wu et al. adapted a similar reactor design for CO_2 photoreduction using WO_3 as an oxidation catalyst and $CuAlGaO_4$ or Rh doped $SrTiO_3$ as a reduction photocatalyst [120].

CO_2 photoreduction over ruthenium dye-sensitized TiO_2-based catalysts under concentrated sunlight has been rendered by Nguyen et al. [121]. A solar concentrator was used to provide the concentrated sunlight. It consisted of a series of reflecting surface which gathered large area light into a focus zone (Fig. 9). As sunlight is the preferable energy provider for this technology, the solar concentrator is beneficial for boosting the technology further.

In summary, the fluidised batch photoreactor is still the most commonly used photoreactor. Both the top and inner illuminated photoreactor are equally popular. The actual design in different research group may be varied slightly, for example, some equip an inferred filter to remove the heat, others use water bath to maintain the reactor temperature. Although advancing reactor design has demonstrated an alternative way to optimize the photoconversion efficiency, this field has not been extensively investigated. Only limited literatures on reactor design have been published so far. It seems an efficient and appropriate reactor's design is still at its fancy stage. On the other hand, a fluidised batch photoreactor can provide a simple environment to scan different photocatalysts in practice.

7. Conclusion

Tackling global warming and fuel crisis is one of the key challenges in this century. Amongst all the techniques to be used for carbon dioxide reduction, photocatalytic CO_2 conversion has its unique advantages that it solely utilises the most abundant solar energy which should not increase CO_2 emission. This technology not only provides an alternative way to produce the sustainable fuels, but also convert the waste CO_2 into valuable chemicals, which is important for keeping our environment clean and development sustainable. There are limitations in the process of CO_2 photoreduction and various strategies have been developed to overcome them. However, more efforts are required to improve the efficiency of the photoreduction reaction. The development of the novel heterostructured photocatalysts with considerable activity, high reaction selectivity for CO_2 reduction and stability is extremely urgent. The crucial role of co-catalysts should be further investigated and the mechanism of the photochemical process is little understood, which limits the reaction efficiency and requires large efforts. In parallel, the efficient photoreactor and reaction system engineering are important but with limited success up to now. In total the technology is rather challenging, thus huge amount of effort should be put into searching a low-cost and robust artificial photocatalyst, understanding the underlying chemical processes and designing an efficient reaction system.

Acknowledgments

Financial support from the EPSRC (EP/H046380/1) is gratefully acknowledged. Junwang Tang and Majeda Khraisheh are thankful for a grant from the Qatar National Research Fund under its National Priorities Research Program award number NPRP 09-328-2-122. Its contents are solely the responsibility of the authors and do not necessarily represent the official views of the Qatar National Research fund.

References

[1] S.C. Roy, O.K. Varghese, M. Paulose, C.A. Grimes, ACS Nano 4 (2010) 1259–1278.
[2] IPCC, Climate Change 2007, Contribution of Working Group 2 to the Fourth Assessment, 2007.
[3] H. Khatib, Energy Policy 48 (2012) 737–743.
[4] (a) T. Yui, Y. Tamaki, K. Sekizawa, O.I. Abstract, Top Curr. Chem. 303 (2011) 151–184;
(b) J. Tang, S. Dai, J.A. Darr, Int. J. Photoenergy (2012), art. no. 580746.
[5] C.D. Windle, R.N. Perutz, Coord. Chem. Rev. 256 (2012) 2562–2570.
[6] Y. Qu, X. Duan, J. Mater. Chem. 22 (2012) 16171–16181.
[7] T.F. Hurst, T.T. Cockerilla, N.H. Florin, Energy Environ. Sci. 5 (2012) 7132–7150.
[8] C. Costentin, M. Robert, J. Saveant, Chem. Soc. Rev. 42 (2013) 2423.
[9] A.T. Najafabadi, Int. J. Energy Res. 37 (2013) 485–499.
[10] H. Jhong, S. Ma, P. Kenis, Curr. Opin. Chem. Eng. 2 (2013) 191–199.
[11] S.N. Habisreutinger, L. Schmidt-Mende, J. Stolarczyk, Angew. Chem. Int. Ed. 52 (2013) 2–39.
[12] V. Indrakanti, J. Kubickib, H. Schobert, Energy Environ. Sci. 2 (2009) 745–758.
[13] J.C. Hemminger, R. Carr, G.A. Somorjai, Chem. Phys. Lett. 57 (1978) 100–104.
[14] X. Chen, S. Shen, L. Guo, S. Mao, Chem. Rev. 110 (2010) 6503–6570.
[15] H. Chen, C. Nanayakkara, V. Grassian, Chem. Rev. 112 (2012) 5919–5948.
[16] W. Fan, Q. Zhang, Y. Wang, Phys. Chem. Chem. Phys. 15 (2013) 2632–2649.
[17] P. Kamat, J. Phys. Chem. Lett. 3 (2012) 663–672.
[18] P. Usubharatana, D. McMartin, A. Veawab, P. Tontiwachwuthikul, Ind. Eng. Chem. Res. 45 (2006) 2558–2568.
[19] Z. Li, W. Luo, M. Zhang, J. Feng, Z. Zou, Energy Environ. Sci. 6 (2013) 347.

[20] A. Kubacka, M. Fernandez-García, G. Colon, Chem. Rev. 112 (2012) 1555–1614.
[21] S. Navaln, A. Dhakshinamoorthy, M. Alvaro, H. Garcia, ChemSusChem 6 (2013) 562–577.
[22] H. Zhou, J. Guo, P. Li, T. Fan, D. Zhang, J. Ye, Sci. Rep. 3 (2013) 1–9.
[23] X. Zhang, F. Han, B. Shi, S. Farsinezhad, G.P. Dechaine, K. Shankar, Angew. Chem. Int. Ed. 51 (2012) 12732–12735.
[24] Y. Izumi, Coord. Chem. Rev. 257 (2013) 171–186.
[25] P. Liao, E. Carter, Chem. Soc. Rev. 42 (2013) 2401–2422.
[26] M. Dozzi, E. Selli, J. Photochem. Photobiol. C 14 (2013) 13–28.
[27] M. Pelaez, N. Nolan, S. Pillai, M. Seery, P. Falaras, A. Kontos, P. Dunlop, J. Hamilton, J. Byrne, K. O'Shea, M. Entezari, D. Dionysiou, Appl. Catal. B-Environ. 125 (2012) 331–349.
[28] R. Daghrir, P. Drogui, D. Robert, Ind. Eng. Chem. Res. 52 (2013) 3581–3599.
[29] S. Kumar, L. Devi, J. Phys. Chem. A 115 (2011) 13211–13241.
[30] M. Rauf, M. Meetani, S. Hisaindee, Desalination 276 (2011) 13–27.
[31] H. Parka, Y. Parkb, W. Kimb, W. Choib, J. Photochem. Photobiol. C 15 (2013) 1–20.
[32] H. Zhang, G. Chen, D. Bahnemann, J. Mater. Chem. 19 (2009) 5089–5121.
[33] Y. Wang, Q. Wang, X. Zhan, F. Wang, S. Muhammad, J. He, Nanoscale (2013), http://dx.doi.org/10.1039/C3NR01577G.
[34] R. Selinsky, Q. Ding, M. Faber, J. Wright, S. Jin, Chem. Soc. Rev. 42 (2013) 2963–2985.
[35] C. Windle, R. Perutz, Coord. Chem. Rev. 256 (2012) 2562–2570.
[36] A.D. Handoko, K. Li, J. Tang, Curr. Opin. Chem. Eng. 2 (2013) 200–206.
[37] J. Tang, J. Durrant, D. Klug, J. Am. Chem. Soc. 130 (2008) 13885–13891.
[38] J. Tang, A.J. Cowan, J.R. Durrant, D.R. Klug, J. Phys. Chem. C 115 (2011) 3143–3150.
[39] A.D. Handoko, J. Tang, Int. J. Hydrogen Energy 38 (2013) 13017–13022.
[40] T. Inoue, A. Fujishima, S. Konishi, K. Honda, Nature 277 (1979) 637–638.
[41] X. Li, J. Chen, H. Li, J. Li, Y. Xu, Y. Liu, J. Zhou, J. Nat. Gas Chem. 20 (2011) 413–417.
[42] J. Mao, T. Peng, X. Zhang, K. Li, L. Ye, L. Zan, Catal. Sci. Technol. 3 (2013) 1253–1260.
[43] L. Liu, H. Zhao, J.M. Andino, Y. Li, ACS Catal. 2 (2012) 1817–1828.
[44] L. Chen, M. Graham, G. Li, D. Gentner, N. Dimitrijevic, K. Gray, Thin Solid Films 517 (2009) 5641–5645.
[45] R. Devan, R. Patil, J. Lin, Y. Ma, Adv. Funct. Mater. 22 (2012) 3326–3370.
[46] K. Yu, W. Yu, M. Ku, Y. Liou, S. Chien, Appl. Catal. B-Environ. 84 (2008) 112–118.
[47] Q. Zhang, W. Han, Y. Hong, J. Yu, Catal. Today 148 (2009) 335–340.
[48] B. Vijayan, N. Dimitrijevic, T. Rajh, K. Gray, J. Phys. Chem. 114 (2010) 12994–13002.
[49] K. Schultea, P. DeSariob, K. Gray, Appl. Catal. B-Environ. 97 (2010) 354–360.
[50] O.K. Varghese, M. Paulose, T.J. LaTempa, C.A. Grimes, Nano Lett. 9 (2009) 731–737.
[51] X. Zhang, F. Han, B. Shi, S. Farsinezhad, G.P. Dechaine, K. Shankar, Angew. Chem. Int. Edit. 51 (2012) 12732–12735.
[52] J. Tan, Y. Fernandez, D. Liu, M. Maroto-Valer, J. Bian, X. Zhang, Chem. Phys. Lett. 531 (2012) 149–154.
[53] X. Li, Z. Zhuang, W. Li, H. Pan, Appl. Catal. A-Gen. 429–430 (2012) 31–38.
[54] W. Li, D. Zhao, Chem. Commun. 49 (2013) 943.
[55] N. Ulagappan, H. Frei., J. Phys. Chem. A 104 (2000) 7834.
[56] M. Anpo, K. Chiba, J. Mol. Catal. 74 (1992) 207.
[57] M. Anpo, H. Yamashita, Y. Ichihashi, Y. Fujii, M. Honda, J. Phys. Chem. B 101 (1997) 2632.
[58] W. Lin, H. Han, H. Frei, J. Phys. Chem. B 108 (2004) 18269.
[59] P. Tran, L. Wong, J. Barber, J. Loo, Energy Environ. Sci. 5 (2012) 5902.
[60] Y. Liu, B. Huang, Y. Dai, X. Zhang, X. Qin, M. Jiang, M.-H. Whangbo, Catal. Commun. 11 (2009) 210–213.
[61] Z.Y. Wang, H.C. Chou, J.C.S. Wu, D.P. Tsai, G. Mul, Appl. Catal. A-Gen. 380 (2010) 172–177.
[62] K. Sayama, H. Arakawa, J. Phys. Chem. 97 (1993) 531–533.
[63] T. Tanaka, Y. Kohno, S. Yoshida, Res. Chem. Intermed. 26 (2000) 93–101.
[64] Y. Kohno, T. Tanaka, T. Funabiki, S. Yoshida, PCCP 2 (2000) 5771.
[65] C. Lo, C.-H. Hung, C.-S. Yuan, J.-F. Wu, Sol. Energy Mater. Sol. Cells 91 (2007) 1765–1774.
[66] Y. Kohno, T. Tanaka, T. Funabiki, S. Yoshida, PCCP 2 (2000) 2635–2639.
[67] Y. Kohno, T. Tanaka, T. Funabiki, S. Yoshida, PCCP 2 (2000) 5302–5307.
[68] Y. Tanaka, S. Kohno, Yoshida, Res. Chem. Intermed. 26 (2000) 93–101.
[69] K. Iizuka, T. Wato, Y. Miseki, K. Saito, A. Kudo, J. Am. Chem. Soc. 133 (2011) 20863–20868.
[70] K. Xie, N. Umezawa, N. Zhang, P. Reunchan, Y. Zhang, J. Ye, Energy Environ. Sci. 4 (2011) 4211–4219.
[71] H. Shi, T. Wang, J. Chen, C. Zhu, J. Ye, Z. Zou, Catal. Lett. 141 (2011) 525–530.
[72] S.C. Yan, S.X. Ouyang, J. Gao, M. Yang, J.Y. Feng, X.X. Fan, L.J. Wan, Z.S. Li, J.H. Ye, Y. Zhou, Z.G. Zou, Angew. Chem. Int. Ed. 49 (2010) 6400–6404.
[73] Q. Liu, Y. Zhou, J.H. Kou, X.Y. Chen, Z.P. Tian, J. Gao, S.C. Yan, Z.G. Zou, J. Am. Chem. Soc. 132 (2010) 14385–14387.
[74] B.J. Ma, F.Y. Wen, H.F. Jiang, J.H. Yang, P.L. Ying, C. Li, Catal. Lett. 134 (2010) 78–86.
[75] H. Park, J. Choi, K. Choi, D. Lee, J. Kang, J. Mater. Chem. 22 (2012) 5304–5307.
[76] H. Tsuneoka, K. Teramura, T. Shishido, T. Tanaka, J. Phys. Chem. C 114 (2010) 8892–8898.
[77] K. Teramura, S.-i. Okuoka, H. Tsuneoka, T. Shishido, T. Tanaka, Appl. Catal. B-Environ. 96 (2010) 565–568.
[78] H. Kato, A. Kudo, J. Phys. Chem. B 105 (2001) 4285–4292.
[79] K. Li, A.D. Handoko, M. Khraisheh, J. Tang, ACS Catal. (2013), In revision.
[80] Y. Matsumoto, M. Obata, J. Hombo, J. Phys. Chem. 98 (1994) 2950–2951.
[81] K. Tennakone, A.H. Jayatissa, S. Punchihewa, J. Photochem. Photobiol. A 49 (1989) 369–375.
[82] H. Li, Y. Lei, Y. Huang, Y. Fang, Y. Xu, L. Zhu, X. Li, J. Nat. Gas Chem. 20 (2011) 145–150.
[83] A. Paracchino, V. Laporte, K. Sivula, M. Grätzel, E. Thimsen, Nat. Mater. 10 (2011) 456.
[84] Z. Zhang, R. Dua, L. Zhang, H. Zhu, H. Zhang, P. Wang, ACS Nano 7 (2013) 1709–1717.
[85] Z.G. Zou, J.H. Ye, K. Sayama, H. Arakawa, Nature 414 (2001) 625–627.
[86] P. Pan, Y. Chen, Catal. Commun. 8 (2007) 1546–1549.
[87] H. Chen, H. Chou, J. Wu, H. Lin, J. Mater. Res. 23 (2008) 1364–1370.
[88] Y. Liu, B. Huang, Y. Dai, X. Zhang, X. Qin, M. Jiang, M. Whangbo, Catal. Commum. 11 (2009) 210–213.
[89] L. Jia, J. Li, W. Fang, Catal. Commun. 11 (2009) 87–90.
[90] S. Sato, T. Morikawa, S. Saeki, T. Kajino, T. Motohiro, Angew. Chem. Int. Ed. 49 (2010) 5101–5105.
[91] T. Suzuki, T. Nakamura, S. Saeki, Y. Matsuoka, H. Tanaka, K. Yano, T. Ajino, T. orikawa, J. Mater. Chem. 22 (2012) 24584.
[92] X. Lv, W. Fu, C. Hu, Y. Chen, W. Zhou, RSC Adv. 3 (2013) 1753–1757.
[93] W. Tu, Y. Zhou, Q. Liu, S. Yan, S. Bao, X. Wang, M. Xiao, Z. Zou, Adv. Funct. Mater. 23 (2013) 1743–1749.
[94] W. Tu, Y. Zhou, Q. Liu, Z. Tian, J. Gao, X. Chen, H. Zhang, J. Liu, Z. Zou, Adv. Funct. Mater. 22 (2012) 1215–1221.
[95] Y. Liang, B. Vijayan, K. Gray, M. Hersam, Nano Lett. 11 (2011) 2865–2870.
[96] G.Q. Li, T. Kako, D.F. Wang, Z.G. Zou, J.H. Ye, J. Phys. Chem. Solids 69 (2008) 2487–2491.
[97] A. Yamakata, T. Ishibashi, H. Onishi, J. Phys. Chem. B 105 (2001) 7258–7262.
[98] W. Wang, W. An, B. Ramalingam, S. Mukherjee, D.M. Niedzwiedzki, S. Gangopadhyay, P. Biswas, J. Am. Chem. Soc. 134 (2012) 11276–11281.
[99] Q. Zhai, S. Xie, W. Fan, Q. Zhang, Y. Wang, W. Deng, Y. Wang, Angew. Chem. Int. Ed. 52 (2013) 5776–5779.
[100] K. Adachi, K. Ohta, T. Mizuno, Solar Energy 53 (1994) 187–190.
[101] H. Yamashita, H. Nishiguchi, N. Kamada, M. Anpo, Y. Teraoka, H. Hatano, S. Ehara, K. Kikui, L. Palmisano, A. Sclafani, M. Schiavello, M.A. Fox, Res. Chem. Intermed. 20 (1994) 815–823.
[102] R.L. Cook, R.C. Macduff, A.F. Sammells, J. Electrochem. Soc. 135 (1988) 3069–3070.
[103] Q. Zhang, T. Gao, J.M. Andino, Y. Li, Appl. Catal. B: Environ. 123–124 (2012) 257–264.
[104] A.A. Peterson, F. Abild-Pedersen, F. Studt, J. Rossmeisl, J.K. Norskov, Energy Environ. Sci. 3 (2010) 1311–1315.
[105] J.C.S. Wu, Catal. Surv. Asia 13 (2009) 30–40.
[106] D. Sui, X. Yin, H. Dong, S. Qin, J. Chen, W. Jiang, Catal. Lett. 142 (2012) 1202–1210.
[107] L. Jiang, Q.Z. Wang, C.L. Li, J.A. Yuan, W.F. Shangguan, Int. J. Hydrogen Energy 35 (2010) 7043–7050.
[108] M.W. Kanan, D.G. Nocera, Science 321 (2008) 1072–1075.
[109] D. Wang, R. Li, J. Zhu, J. Shi, J. Han, X. Zong, C. Li, J. Phys. Chem. C 116 (2012) 5082–5089.
[110] M. Nishikawa, S. Hiura, Y. Mitani, Y. Nosaka, J. Photochem. Photobiol. A 262 (2013) 52–56.
[111] A. Kudo, H. Kato, Chem. Phys. Lett. 331 (2000) 373–377.
[112] M. Barroso, A.J. Cowan, S.R. Pendlebury, M. Graetzel, D.R. Klug, J.R. Durrant, J. Am. Chem. Soc. 133 (2011) 14868–14871.
[113] S. Xie, Y. Wang, Q. Zhang, W. Fan, W. Deng, Y. Wang, Chem. Commun. 49 (2013) 2451–2453.
[114] X. Zong, H. Yan, G. Wu, G. Ma, F. Wen, L. Wang, C. Li, J. Am. Chem. Soc. 130 (2008) 7176.
[115] X. Zong, J. Han, G. Ma, H. Yan, G. Wu, C. Li, J. Phys. Chem. C 115 (2011) 12202–12208.
[116] S.W. Seo, S. Park, H.-Y. Jeong, S.H. Kim, U. Sim, C.W. Lee, K.T. Nam, K.S. Hong, Chem. Commun. 48 (2012) 10452–10454.
[117] G. Liu, N. Hoivik, K. Wang, H. Jakobsen, Sol. Energy Mater. Sol. Cells 105 (2012) 53–68.
[118] O. Ola, M. Maroto-Valer, D. Liu, S. Mackintosh, C.-W. Lee, J.C. Wu, Appl. Catal. B-Environ. 126 (2012) 172–179.
[119] S. Ichikawa, R. Doi, Catal. Today 27 (1996) 271–277.
[120] W. Lee, C. Liao, M. Tsai, C. Huang, J.C.S. Wu, Appl. Catal. B-Environ. 132–133 (2013) 445–451.
[121] T. Nguyen, J.C.S. Wu, C.-H. Chiou, Catal. Commun. 9 (2008) 2073–2076.